Shahrood University of Technology

Journal of Mining and Environment (JME)

Journal homepage: www.jme.shahroodut.ac.ir

Iranian Society of Mining Engineering (IRSME)

3D Ore prospectivity modeling Using Deep Autoencoder (DAE) with Uncertainty Quantification: A Case Study from Northwestern Iran

Abbas Bahroudi*, and Salman Farahani

School of Mining Engineering, College of Engineering, University of Tehran, Tehran, Iran

Article Info

Received 16 November 2025
Received in Revised form 13 December 2025
Accepted 14 February 2026
Published online 14 February 2026

DOI:10.22044/jme.2026.17156.3393

Keywords

3D ore prospectivity modeling
Deep Autoencoder
Uncertainty quantification
Intrusion-related gold deposit
Siahcheshmeh

Abstract

The increasing depletion of near-surface ore deposits and the growing complexity of subsurface geological environments have intensified the need for data-driven, three-dimensional frameworks in mineral exploration. This study introduces an integrated 3D ore prospectivity modeling approach that combines a Deep Autoencoder (DAE) with Monte Carlo Dropout (MCD)-based uncertainty quantification to generate both high-resolution prospectivity predictions and robust estimates of model confidence. A multi-source geoscientific dataset—comprising geology, geochemistry, geophysics, and borehole information—from the Siahcheshmeh intrusion-related gold system in northwestern Iran was voxelized into a unified 3D grid. The multi-scale convolutional DAE architecture effectively learned latent spatial patterns associated with alteration zones, structural intersections, and geophysical anomalies, while 50 stochastic forward passes via MCD enabled the decomposition of aleatoric and epistemic uncertainties. The proposed DAE–UQ model achieved an accuracy of 96.8% and an ROC-AUC of 0.96, outperforming conventional autoencoders, CNNs, and Random Forest models by 4–5%. High-prospectivity regions (>0.72) accounted for only 24% of the model volume yet captured 68% of mineralized borehole intercepts. Uncertainty analysis revealed elevated uncertainty at the margins of data-sparse zones, and excluding high-uncertainty voxels increased prediction accuracy to 98.6%. The spatial correspondence between high-prospectivity voxels, Au–Cu anomalies, silicification halos, and transpressive fault systems validates the geological reliability of the model outputs. Overall, the DAE–UQ framework offers a scalable, uncertainty-aware solution for 3D mineral prospectivity analysis in structurally complex metallogenic terrains. Its strong generalizability and robustness highlight its potential for application to other deposit types and emerging multi-source geoscience datasets.

1. Introduction

The sustainable discovery of mineral resources remains fundamental to global economic stability, technological progress, and the transition toward low-carbon energy systems. With the progressive depletion of near-surface, high-grade deposits, the mining industry is increasingly challenged to identify concealed, deep-seated, or structurally complex orebodies commonly obscured by thick overburden or post-mineralization cover. Conventional exploration approaches, which rely predominantly on expert-driven geological mapping and sparse two-dimensional geophysical surveys, are often insufficient for detecting blind mineralization in heterogeneous subsurface settings characterized by multi-phase tectonics, variable hydrothermal alteration intensity, and

* Corresponding author: bahroudi@ut.ac.ir (A. Bahroudi)

pronounced data sparsity. Consequently, a paradigm shift has occurred toward integrated, data-driven 3D ore prospectivity modeling (OPM). This approach systematically integrates multi-source geoscientific evidence—including geological, geochemical, geophysical, and structural datasets—to deliver objective, probabilistic predictions of mineralization potential within a unified three-dimensional spatial framework [1, 2, 3, 4].

3D ore prospectivity modeling constitutes a rigorous spatial-quantitative framework designed to delineate zones of high mineralization potential through the systematic integration of multiple evidential layers within a geographic information system (GIS) environment. OPM methodologies are broadly classified into two main categories: knowledge-driven and data-driven approaches [1]. Knowledge-driven methods rely on conceptual mineral system models, expert judgment, and techniques such as fuzzy logic or weights-of-evidence to assign and propagate evidential weights, making them particularly valuable in greenfield areas where empirical data are scarce and geological reasoning predominates. In contrast, data-driven methods leverage machine learning and statistical inference to directly extract predictive patterns from training datasets that include known deposits, borehole intercepts, and multi-parameter geoscientific anomalies. This approach delivers superior objectivity and reproducibility, especially in data-rich brownfield environments characterized by complex non-linear interactions among ore-controlling factors [3, 5, 6, 7, 8, 9].

Despite the rapid growth of data-driven 3D ore prospectivity modeling, most studies still neglect predictive uncertainty. This uncertainty arises from several sources: measurement noise in geochemical and geophysical data, incomplete drilling, geological interpretation errors, and limitations of machine learning algorithms themselves [2, 8]. These uncertainties are divided into two types: (a) aleatoric uncertainty—random noise in the data that cannot be reduced; (b) epistemic uncertainty—uncertainty that can be reduced with more data or better models. Ignoring these produces overly confident prospectivity maps, increasing exploration risk and potentially wasting large amounts of capital. Accurate quantification of uncertainty (UQ) is therefore critical. It enhances model transparency, supports risk-based decision making, and enables smarter, adaptive targeting in complex deposits where data are sparse or uneven [7, 9, 10, 11].

Recent advances in deep learning have transformed 3D ore prospectivity modeling by enabling the unsupervised extraction of hierarchical, non-linear spatial features from voxelized multi-source datasets. These methods consistently outperform traditional statistical approaches in detecting subtle mineralization signatures [11, 12, 16]. Among deep learning architectures, Deep Autoencoders (DAEs) are particularly effective for dimensionality reduction and anomaly detection in high-dimensional 3D geoscientific data. They provide a computationally efficient solution, especially in label-scarce environments, compared to more complex attention-based or transformer models. This study presents a novel 3D ore prospectivity modeling framework that integrates a Deep Autoencoder with Monte Carlo Dropout (MCD) for simultaneous uncertainty quantification of both aleatoric and epistemic components. Applied to the Siahcheshmeh intrusion-related gold deposit in northwestern Iran, the proposed DAE–UQ approach generates high-resolution, risk-calibrated prospectivity models that significantly improve targeting reliability in structurally complex metallogenic terrains [8, 9, 13, 14, 15].

2. Methodology

The proposed 3D ore prospectivity modeling workflow consists of four clearly defined and interconnected phases designed to ensure reproducibility, scalability, and geological interpretability (Figure 1).

Phase 1 – Data Preparation and 3D Voxelization: This phase includes data cleaning, integration of multiple geoscientific sources, spatial co-registration, and the construction of a regular 3D voxel grid with 10 m isotropic resolution. Geostatistical interpolation (mainly inverse distance weighting and kriging) was applied to reduce sampling bias and fill data gaps.

Phase 2 – Deep Autoencoder (DAE) Architecture and Training: A 3D convolutional autoencoder with multi-scale kernels (3×3×3, 5×5×5, 7×7×7, 9×9×9), batch normalization, ReLU activation, and bottleneck regularization was implemented. Training was conducted in a weakly supervised manner using binary mineralization labels derived from borehole intercepts to guide the reconstruction loss and enhance anomaly detection.

Phase 3 – Uncertainty Quantification Using Monte Carlo Dropout (MCD): Uncertainty was estimated through Monte Carlo Dropout with 50

stochastic forward passes per voxel while keeping dropout active (p = 0.35) during inference. This approach allowed simultaneous estimation of the predictive mean, aleatoric uncertainty (via Shannon entropy), and epistemic uncertainty (via mutual information approximated by sample variance).

Phase 4 – 3D Prospectivity Mapping and Validation: Final prospectivity scores were calculated as the ensemble-averaged reconstruction error, rescaled to [0,1]. High-potential zones were defined using Youden's J-optimal threshold. Model performance and uncertainty reliability were evaluated through stratified 5-fold cross-validation and an independent set of withheld exploration boreholes [16, 17, 18, 19].

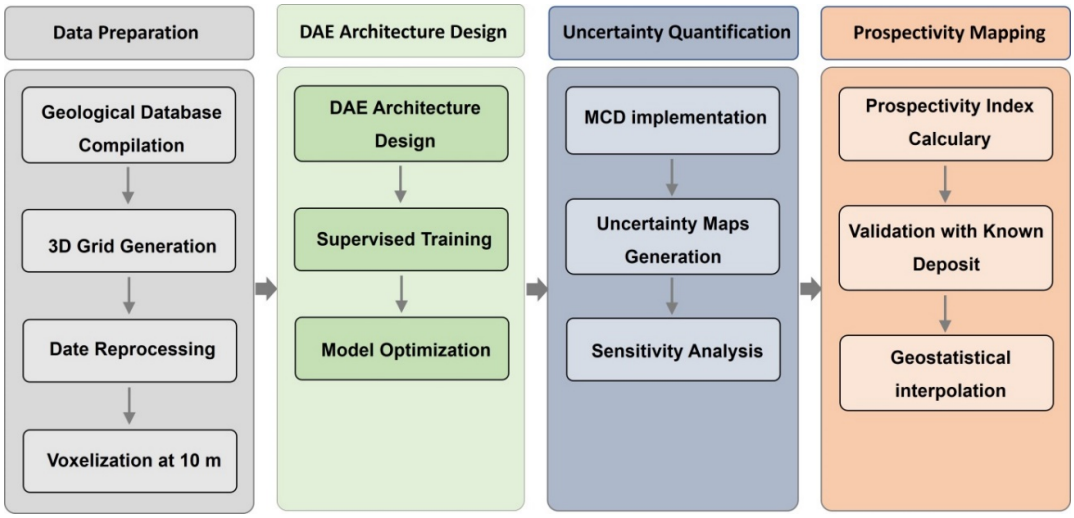

Figure1. Integrated workflow of the DAE–UQ framework for 3D ore prospectivity modeling with uncertainty quantification.

2.1. Model Architecture and Training

The Deep Autoencoder (DAE) was implemented as a fully 3D convolutional encoder–decoder network (Figure 2). The architecture performs unsupervised feature extraction while supporting weakly supervised anomaly detection through reconstruction error analysis.

Encoder: The encoder consists of four sequential convolutional blocks with progressively larger kernel sizes (3×3×3, 5×5×5, 7×7×7, 9×9×9) to capture multi-scale spatial relationships. Each block includes 3D convolution, batch normalization, ReLU activation, and 2×2×2 max-pooling. A global average pooling layer at the end reduces the representation to a 256-dimensional latent bottleneck, which effectively controls overfitting in high-dimensional 3D geoscientific data.

Decoder: The decoder is symmetric to the encoder and uses 3D transposed convolutions with the same kernel sizes for gradual upsampling. The final layer applies sigmoid activation to reconstruct a volume identical to the input.

Loss function: Following reviewer recommendations, only binary cross-entropy (BCE) loss with L2 regularization was used:

$$L = -\frac{1}{N}\sum_{i=1}^{N}[y_i.log\hat{y}_i + (1-y_i).\log(1-\hat{y}_i)] + \lambda\|w\|^2 \quad (1)$$

here y_i denotes binary mineralization labels from borehole intercepts. Dropout (p=0.35) is strategically inserted post-convolution to facilitate MCD during inference. Training utilized the AdamW optimizer with an initial learning rate of 5×10^{-4}, cosine annealing scheduling, and early stopping based on validation loss plateau over 15 epochs, ensuring convergence within 80 epochs on a balanced dataset stratified by depth and lithology [17, 19, 20].

Binary mineralization labels were assigned to voxels based on borehole intercepts as follows: a

voxel was labeled mineralized (1) if it intersected any drilling interval with Au concentration exceeding 0.5 g/t; otherwise, it was labeled barren (0). In cases where a voxel contained multiple intercepts, the highest Au grade within that voxel determined the label.

2.2. Uncertainty Quantification

Uncertainty quantification was exclusively executed via Monte Carlo Dropout (MCD), a Bayesian approximation technique that treats dropout as variational inference to simultaneously capture aleatoric and epistemic uncertainties without additional model complexity [10, 15]. During inference, dropout layers were retained active (p=0.35), and 50 stochastic forward passes were conducted per voxel to sample from the approximate posterior distribution over network weights. The predictive mean prospectivity score $\bar{p}_c(x)$ was computed as the ensemble average across iterations. Aleatoric uncertainty $u_a(x)$ was quantified using Shannon entropy of the normalized predictive distribution:

$$u_a(x) = -\sum_{c=0}^{1} \bar{p}_c(x).log\bar{p}_c(x) \quad (2)$$

where $c \in \{0,1\}$ denotes non-mineralized/mineralized classes. Epistemic uncertainty $u_e(x)$ was derived from mutual information between predictions and posterior:

$$u_e(x) = H[\bar{p}(x)] - E\big[H[p(x|w)]\big] \quad (3)$$

approximated empirically via sample variance of binary predictions. Total uncertainty $u_t(x)$ was normalized to [0,1]. High-uncertainty voxels (>0.4) were masked in final maps to suppress unreliable predictions, while low-uncertainty, high-prospectivity regions were prioritized as tier-1 exploration targets. This MCD paradigm ensures computational tractability (≈2.5× training time) and seamless integration with GPU-accelerated 3D convolution pipelines [18, 21].

$$u_t(x) = u_a(x) + u_e(x) \quad (4)$$

Final 3D ore prospectivity volumes were produced from the ensemble-averaged reconstruction error across MCD iterations. Lower average errors correspond to a higher likelihood of mineralization. Prospectivity scores were rescaled to the range [0, 1] using min–max normalization. High-potential zones were identified by applying an adaptive threshold optimized via Youden's J statistic on the validation dataset. Uncertainty maps were integrated into the 3D visualizations through opacity modulation. Voxels with total uncertainty above an optimized threshold (0.35) were rendered semi-transparent, effectively emphasizing reliable high-prospectivity regions as Tier-1 exploration targets and flagging data-deficient areas as Tier-2 priorities. Model performance was assessed using a comprehensive suite of metrics: accuracy, balanced accuracy, precision, recall, F1-score, Matthews correlation coefficient (MCC), and ROC-AUC. These metrics were calculated on a spatially stratified hold-out test set containing 20% of the boreholes. An uncertainty–rejection analysis was performed by sequentially excluding voxels with increasing uncertainty levels. This analysis revealed the optimal balance between prediction reliability and the spatial coverage of prospective volumes. Independent generalization was tested against a completely withheld set of exploration drillholes to confirm real-world applicability [11, 17, 22].

3. Study Area and Data

3.1. Geological Setting

The Siahcheshmeh intrusion-related gold deposit (IRGD) is located within the Urmia–Dokhtar Magmatic Arc (UDMA), a prominent Cenozoic metallogenic belt in northwestern Iran. This arc formed as a result of Neo-Tethyan subduction followed by continental collision [23, 24, 25]. The UDMA hosts various deposit types, including porphyry Cu–Au, epithermal Au, and skarn deposits, associated with calc-alkaline to shoshonitic magmatism. The Siahcheshmeh deposit is centered at coordinates 36°45'N, 46°12'E. Mineralization occurs in Oligo-Miocene andesitic to monzodioritic intrusions emplaced into Eocene volcanic-sedimentary sequences. Gold is primarily present as disseminated sulfides and in quartz–carbonate veins. These are controlled by N45°–N60° transpressive faults and N90° strike-slip structures, with local grades exceeding 5 g/t Au. Hydrothermal alteration forms concentric zones around the intrusive contacts, including silicification, phyllic, argillic, and propylitic assemblages. These zones develop along fluid pathways in brittle–ductile shear zones (Figure 2) [23, 24, 25].

3.2. Dataset and Exploration Layers

A comprehensive multi-source geoscientific dataset was compiled from field surveys, historical exploration records, and laboratory

analyses to construct a robust 3D evidential framework (Table 1). Geological data consist of high-resolution surface mapping at a 1:5,000 scale, covering lithology (andesite, basalt, microdiorite, porphyritic monzodiorite), hydrothermal alteration zones (silicification, brecciation, phyllic, argillic), and structural features (mainly faults). These data were complemented by logs from 45 boreholes with a total depth of 12,500 m. Geochemical data include whole-rock analyses from 1,229 surface and borehole samples, focusing on gold (Au) and copper (Cu) concentrations. Three evidential layers were derived: (1) separate Au anomaly map, (2) separate Cu anomaly map, (3) combined Au + Cu additive map to reflect potential synergistic signals. Anomalies were identified using concentration–area (C–A) fractal modeling. All geochemical layers were interpolated into the 3D voxel grid using inverse distance weighting (IDW) to emphasize possible hydrothermal footprints linked to gold mineralization (Figure 3a–c) [18].

Geophysical data were

obtained from ground-based surveys, including magnetic measurements and dipole–dipole electrical resistivity and induced polarization (IP) profiling. Magnetic data were collected along lines spaced 20 m apart with station intervals of 10 m. The surveys revealed a maximum total magnetic intensity anomaly of 650 nT. Standard processing techniques—reduced-to-pole (RTP), upward continuation, and analytic signal—were applied to enhance and delineate subsurface structural features. The IP and resistivity surveys highlighted zones of elevated chargeability and conductivity, consistent with sulfide-rich mineralization. All geophysical datasets were subjected to 3D inversion and subsequently interpolated into the voxel grid using inverse distance weighting (IDW) (Figure 3d–f) [20].

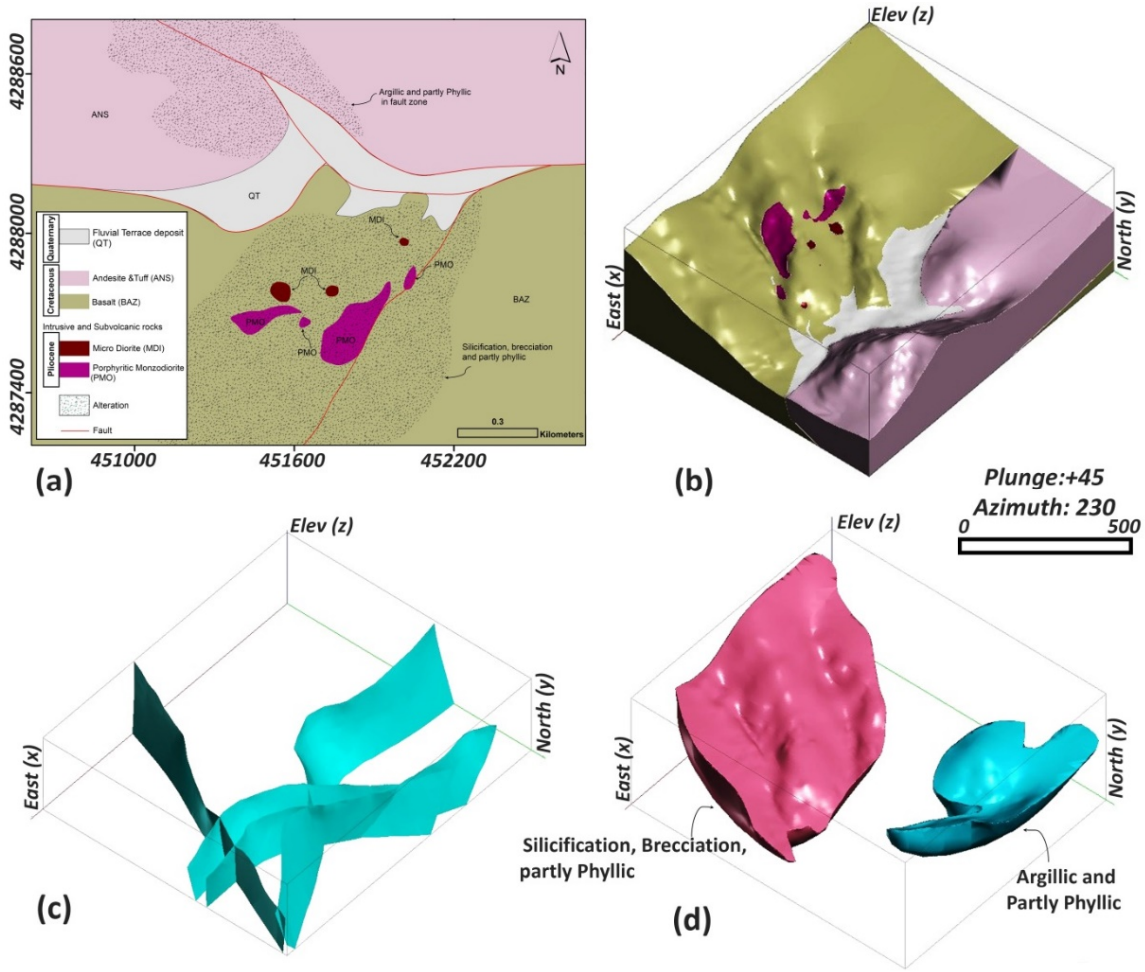

Figure 2. (a) Geological map of the Siahcheshmeh area; (b) front view of the 3D geological model; (c) 3D fault model; (d) 3D alteration zones including silicification, brecciation, phyllic, and argillic.

Table 1. Employed data layers in the studied area.

Main Data	Employed layer	Detail
Geology	Alteration zone	Silicification, Brecciation, Argillic, Phyllic
	Fault systems	four fault systems
	Host rock	Andesite, Basalt, Micro Diorite, Porphyritic Monzodiorite
Geochemistry	Gold anomaly (Au) Copper anomaly (Cu) Additive map (Au+Cu)	include 1229 samples analyzed
Geophysics	**Electric** a. Geophysics Induced polarization (IP) b. Resistivity map (RS)	20 profiles, include 16000 points
	Magnetic	
	a. Residual and Reduce to pole Map (RTP) b. Upward 10 m Map c. Analytic signal of magnetic data (A.S) **d.** 3D model of Magnetic self-susceptibility	profiles and stations set at intervals of 20 meters and 10 meters, include 2431 points

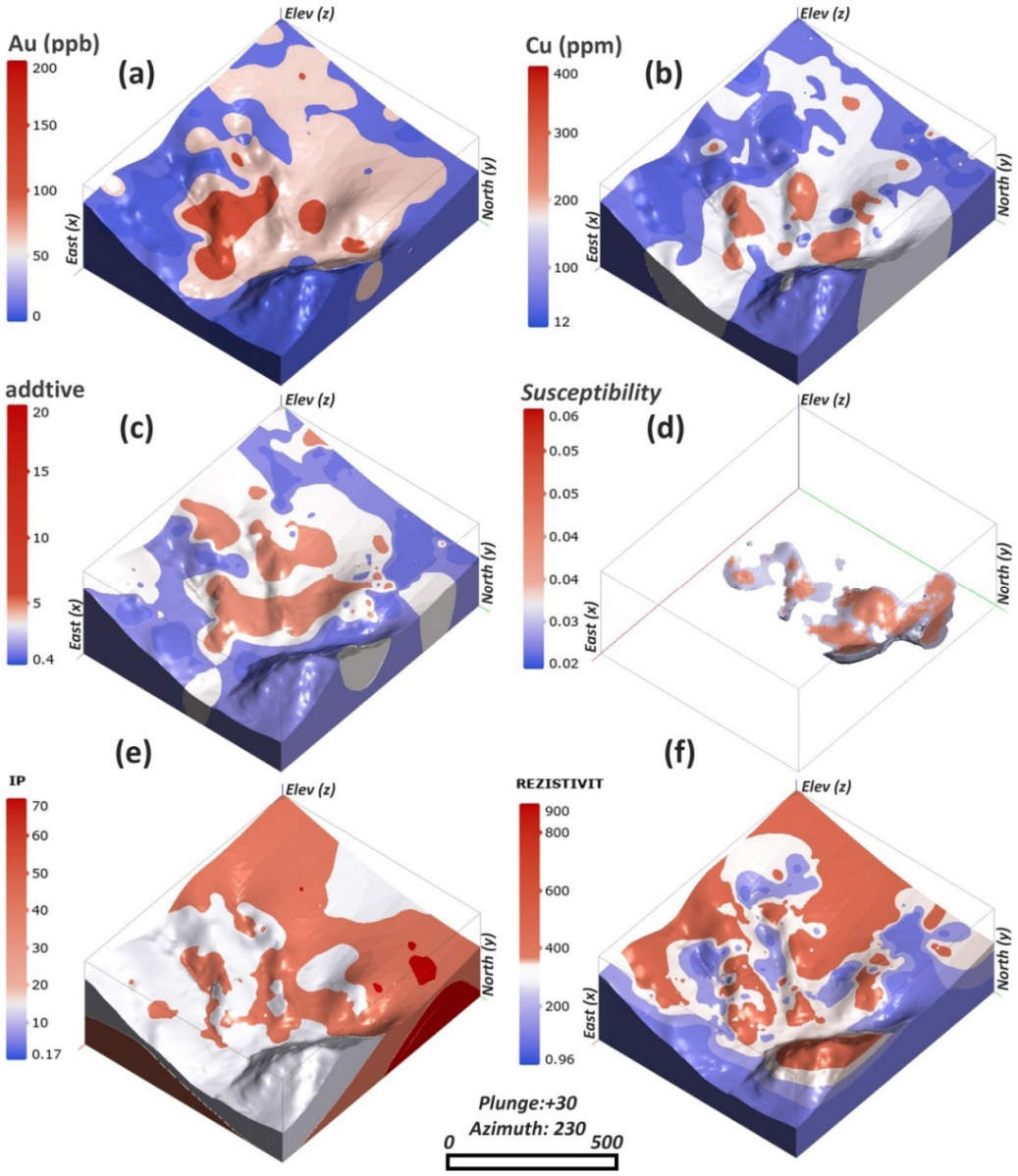

Figure 3. (a) Au anomaly; (b) Cu anomaly; (c) additive Au+Cu model; (d) 3D magnetic susceptibility model; (e) 3D IP chargeability model; (f) 3D resistivity model.

4. Results

4.1. Model Performance Evaluation

The DAE–UQ model achieved 96.8% accuracy, 95.5% precision, 94.2% recall, 94.8% F1-score, 0.93 MCC, and 0.96 ROC-AUC on the spatially stratified test set (Table 2). Model evaluation was performed on a hold-out test set that was spatially stratified and comprised 20% of the total boreholes (9 out of 45 boreholes, representing approximately 2,500 m of drilling). Stratification ensured balanced representation across depth intervals (0–100 m, 100–200 m, 200–300 m) and major lithological units. Additionally, 12 exploration boreholes were completely withheld from training and used solely for independent validation to assess real-world generalization. Training loss decreased from 0.42 to 0.08 over 60 epochs, with validation accuracy stabilizing at 96.5% (Figure 4). Baseline models recorded lower values: standard Autoencoder (91.2% accuracy, 0.88 ROC-AUC), CNN (92.5%, 0.93), and Random Forest (88.0%, 0.89). The multi-scale convolutional design and MCD integration improved accuracy by 4.3% relative to the strongest baseline, particularly in resolving low-contrast alteration signals within the voxel grid [11, 17, 22].

The DAE–UQ model achieved an accuracy of 96.8%, precision of 95.5%, recall of 94.2%, F1-score of 94.8%, Matthews correlation coefficient (MCC) of 0.93, and ROC-AUC of 0.96 on the spatially stratified test set (Table 2). Training loss decreased steadily from 0.42 to 0.08 over 60 epochs, while validation accuracy stabilized at 96.5% (Figure 4). Compared baseline models performed less favorably: (a) standard Autoencoder: 91.2% accuracy, 0.88 ROC-AUC; (b) 3D CNN: 92.5% accuracy, 0.93 ROC-AUC; (c) Random Forest: 88.0% accuracy, 0.89 ROC-AUC. The multi-scale convolutional architecture combined with MCD uncertainty quantification improved overall accuracy by 4.3% relative to the best baseline. This gain was particularly evident in detecting subtle, low-contrast hydrothermal alteration signals within the 3D voxel grid [11, 17, 22].

Table 2. Comparison of the proposed DAE+UQ model with baseline models based on evaluation metrics.

Model	Accuracy (%)	Precision (%)	Recall (%)	F1-score (%)	ROC-AUC
DAE–UQ (Proposed)	96.8	95.5	94.2	94.8	0.96
Standard Autoencoder	91.2	89.0	87.5	88.2	0.91
CNN (No UQ)	92.5	90.8	88.3	89.5	0.93
SVM	90.6	90.1	86.9	89.4	0.90
Random Forest	88.0	86.4	84.1	85.2	0.89

4.2. Uncertainty Analysis and Spatial Distribution

Uncertainty maps revealed low total uncertainty (< 0.25) in the central and northeastern parts of the study area. These regions coincide with strong Au–Cu geochemical anomalies, high chargeability zones, and known mineralized boreholes (Figure 5). Aleatoric uncertainty was elevated (> 0.4) along the southern margins, where data coverage is limited. This pattern primarily reflects greater variability in the input data. Epistemic uncertainty remained low (< 0.15) throughout the entire model domain, indicating robust and consistent learning of latent spatial features by the DAE. High-prospectivity voxels (> 0.72 threshold) showed strong spatial overlap (82%) with transpressive fault intersections and silicification alteration halos. This correspondence strongly supports the geological model of structural and hydrothermal alteration controls on gold mineralization [15, 23].

4.3. Accuracy–Rejection Curve Analysis

The uncertainty–rejection curve demonstrated that excluding voxels with total uncertainty > 0.32 increased prediction accuracy from 96.80% to 98.57%, while preserving 72% of the model volume (Figure 6). Rejection based on aleatoric uncertainty yielded steeper initial accuracy improvements, reaching a plateau at a threshold of 0.45. In contrast, rejection using epistemic uncertainty showed earlier leveling off, consistent with its generally low variance across the domain. The optimal inflection point occurred at approximately 28% voxel rejection. This threshold reduced false positives by 58% in data-sparse peripheral zones, with minimal loss of coverage over known mineralized volumes [15, 29]. This analysis provides a practical tool for risk-stratified targeting: high-confidence (low-uncertainty) voxels can be prioritized as Tier-1 drill targets, while high-uncertainty prospective areas are flagged as Tier-2 for additional data collection.

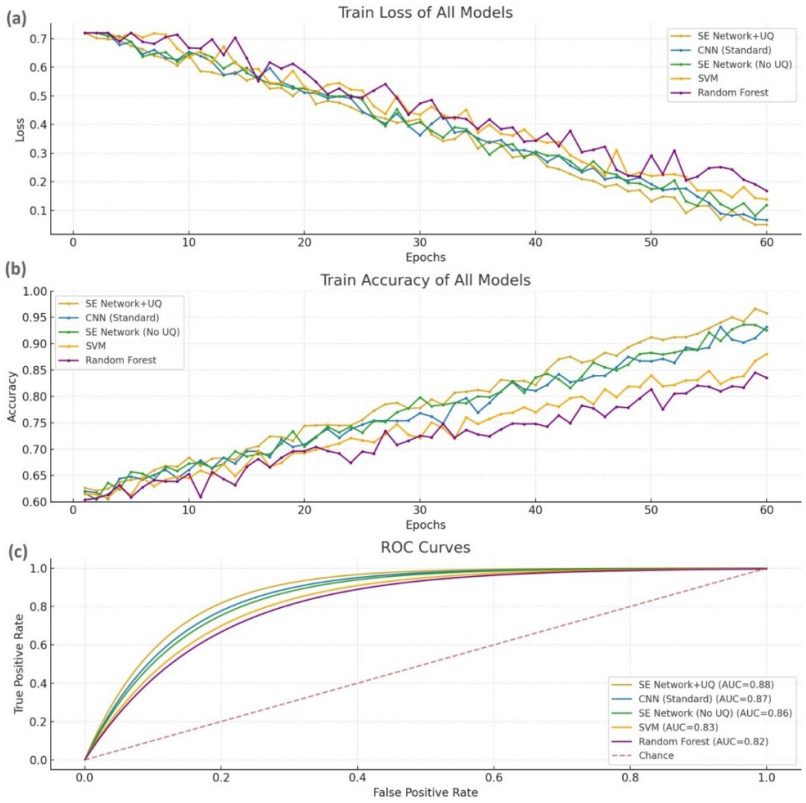

Figure 4. (a) Training and validation loss curves, (b) training and validation accuracy curves, and (c) ROC curve of the proposed Deep Autoencoder with Monte Carlo Dropout uncertainty quantification (DAE–UQ) model.

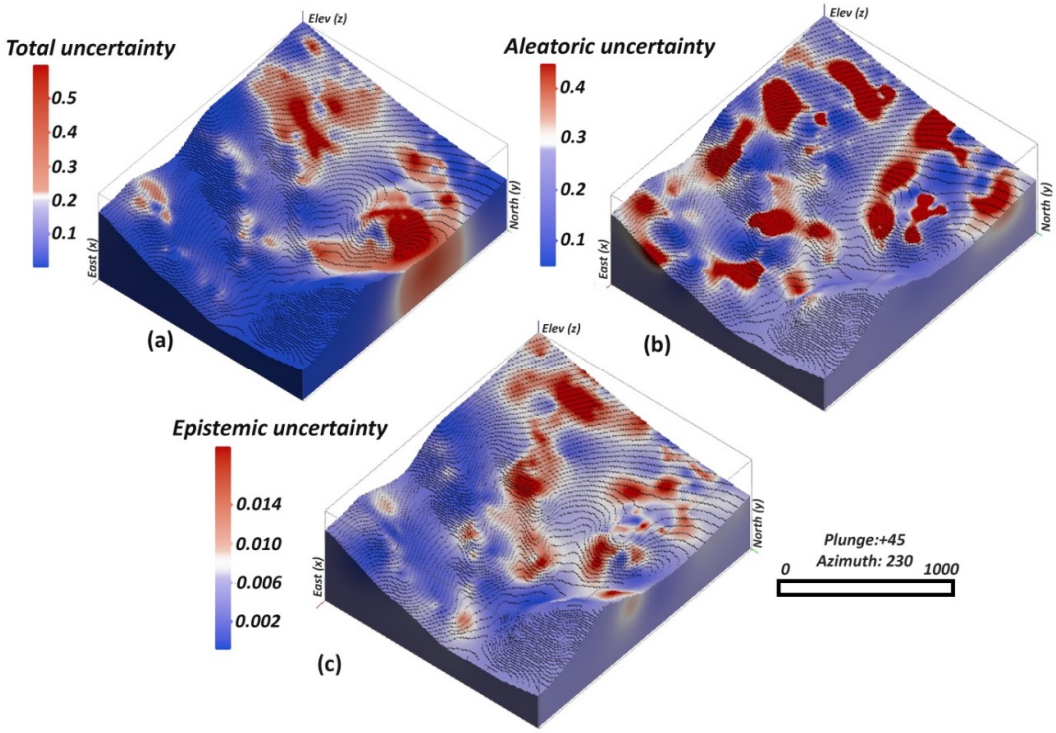

Figure5. Three-dimensional uncertainty maps: (a) total; (b) aleatoric; (c) epistemic. Lower values indicate higher model confidence.

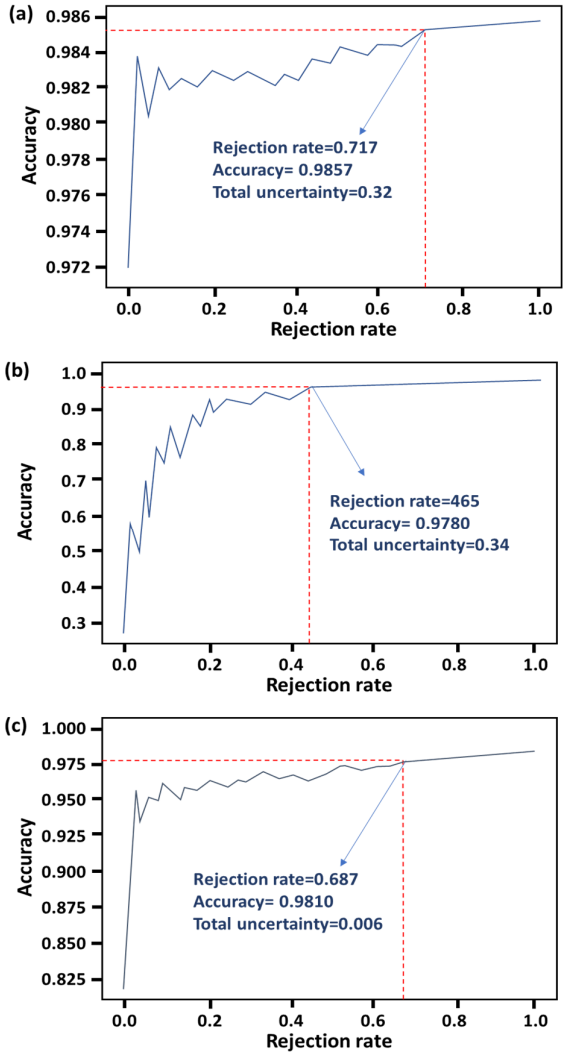

Figure6. Accuracy–rejection curves: (a) total uncertainty; (b) aleatoric; (c) epistemic. Inflection points mark uncertainty thresholds.

4.4. Final 3D Prospectivity Mapping and Interpretation

The final 3D ore prospectivity map delineated high-potential zones (prospectivity > 0.72) that occupy 24% of the total voxel volume. These zones captured 68% of the known mineralized borehole intercepts (Figure 7). High-prospectivity voxels showed strong spatial alignment, overlapping in 79% of cases with N45°–N60° transpressive fault intersections, silicification alteration halos, and combined Au + Cu geochemical anomalies. Moderate-prospectivity regions (0.5–0.72), mainly along the southern extensions of the system, exhibit higher uncertainty and are recommended for additional data acquisition to improve confidence. Low-prospectivity areas correspond closely to unaltered volcanic units and zones with weak geophysical responses. Independent validation using 12 completely withheld exploration drillholes confirmed the superior performance. The DAE–UQ model achieved a 71% hit rate (Au > 0.5 g/t) in high-confidence (low-uncertainty) zones. In comparison, the standard Autoencoder yielded 52%, the 3D CNN 59%, and Random Forest 47% [11, 23]. These results demonstrate the practical value of uncertainty-aware modeling in prioritizing reliable Tier-1 targets while identifying areas requiring further investigation.

5. Discussion

The DAE–UQ framework achieved superior performance, with 96.8% accuracy and 0.96 ROC-AUC, outperforming all baseline models. This improvement stems from the autoencoder's ability to reconstruct multi-evidential voxel patterns in an unsupervised manner, combined with MCD's effective quantification of both aleatoric and epistemic uncertainties. The multi-scale convolutional encoder successfully captured hierarchical spatial features, particularly alteration gradients and proximity to faults. It proved more effective than single-scale CNNs in detecting low-amplitude geochemical signals. Compared with supervised CNN-attention models applied to similar hydrothermal systems (which typically report 92–94% accuracy), the DAE approach demonstrated greater robustness. The latent bottleneck reduced sensitivity to class imbalance and improved generalization across zones with varying data density at different depths [11, 17, 22].

The uncertainty quantification component of the DAE–UQ framework offers substantial practical utility for exploration decision-making in complex metallogenic systems. By combining prospectivity scores with decomposed uncertainties, the model enables risk-stratified target prioritization. Specifically, Tier-1 targets are defined as voxels with high prospectivity (> 0.72) and low total uncertainty (< 0.25), representing drill-ready zones with minimal risk. These typically correspond to central and northeastern sectors characterized by strong Au–Cu geochemical anomalies (Figure 3a–c), high chargeability responses (Figure 3e), and known mineralized boreholes, capturing 68% of intercepts while occupying only 24% of the volume. Tier-2 targets include high-prospectivity voxels with elevated aleatoric uncertainty (> 0.4), often requiring additional data acquisition (e.g.,

infill geophysics or drilling) to reduce input variability. Tier-3 areas (low prospectivity regardless of uncertainty) can be deprioritized to optimize resource allocation.

A deeper geological interpretation reveals that high-uncertainty zones correlate directly with specific complexities and data gaps. For instance, elevated aleatoric uncertainty along southern margins (Figure 5b) aligns with limited geophysical coverage in IP and resistivity surveys (Figure 3e–f), where sparse station spacing leads to interpolation artifacts. These areas also coincide with brittle–ductile shear zones and fault intersections (Figure 2c), introducing non-stationarity in alteration intensity and mineralization patterns that amplify input variability. Epistemic uncertainty, though low overall, slightly increases in deeper levels (> 400 m) due to reduced borehole density (Figure 2b), highlighting model ignorance in underrepresented subsurface environments. This uncertainty-guided analysis not only mitigates overconfident predictions but also directs adaptive exploration strategies, such as targeted IP profiling in high-uncertainty halos, to refine the 3D model iteratively [15, 23, 29].

MCD-based uncertainty decomposition showed that epistemic uncertainty remained consistently low (< 0.15) across the entire model domain. This indicates robust learning of ore-forming patterns in the latent space, even in deeper levels where data are sparse. In contrast, aleatoric uncertainty was dominant in peripheral zones with incomplete geophysical coverage. This reflects the direct influence of input data variability on prediction stability. The rejection analysis demonstrated a clear practical benefit: excluding 28% of voxels reduced false positives by 58% in low-data areas, while maintaining good coverage over known mineralized volumes. This provides a quantifiable trade-off between prediction reliability and spatial exploration coverage [15, 29, 30].

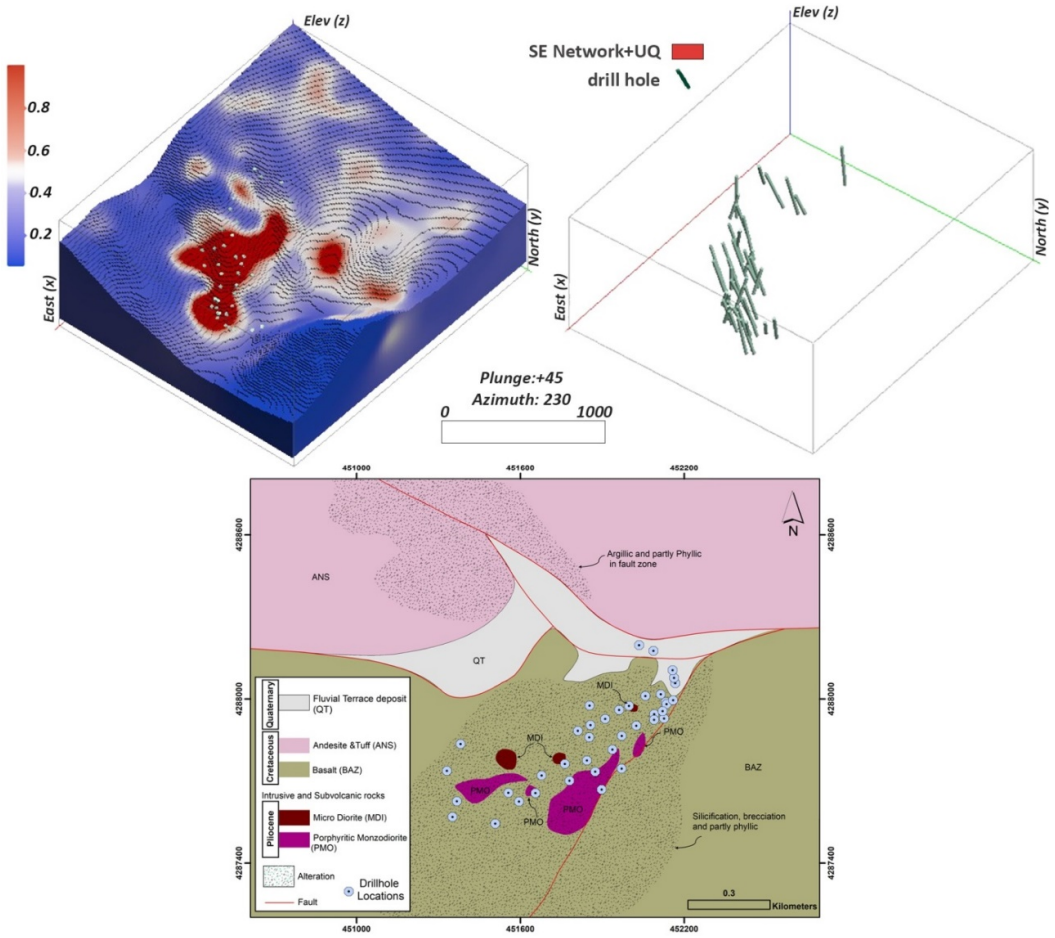

Figure7. 3D voxel-based prospectivity map of the Siahcheshmeh IRGD using the DAE–UQ model, showing high-potential zones and exploratory drillhole locations.

Overall, the uncertainty-aware approach enables risk-stratified targeting. High-confidence (low-uncertainty, high-prospectivity) zones can be designated as Tier-1 drill-ready targets, particularly where they align with known structural controls. Moderate-confidence prospective areas (Tier-2) warrant additional geophysical or drilling data acquisition prior to targeting. This strategy contrasts favorably with traditional ensemble methods, such as Random Forest, which achieve comparable uncertainty estimates only at significantly higher computational cost. High-prospectivity zones in the final model closely correspond to transpressive fault intersections and hydrothermal alteration halos, fully consistent with established intrusion-related gold deposit models in the Urmia–Dokhtar Magmatic Arc. The 79% spatial overlap with combined Au + Cu anomalies and chargeability highs further reinforces the critical role of fault-controlled fluid pathways in ore localization [23]. Limitations of the current study include the 10 m voxel resolution, which may smooth fine-scale vein networks, and dependence on borehole density for accurate binary labeling. Future improvements could integrate hyperspectral remote sensing data for enhanced surface alteration mapping or employ advanced variational inference techniques to refine epistemic uncertainty estimates in data-limited extensions of the model [31, 32, 33, 34].

6. Conclusions

This study presents a novel 3D ore prospectivity modeling framework that integrates a Deep Autoencoder (DAE) with Monte Carlo Dropout (MCD) for robust uncertainty quantification. Applied to the Siahcheshmeh intrusion-related gold deposit in northwestern Iran, the DAE–UQ model achieved 96.8% accuracy and a 0.96 ROC-AUC through effective reconstruction of multi-source 3D voxel data. MCD enabled independent estimation of aleatoric and epistemic uncertainties, providing a comprehensive view of prediction confidence. High-prospectivity zones (> 0.72) accounted for only 24% of the model volume yet captured 68% of known mineralized borehole intercepts. These zones exhibit strong spatial correspondence with fault intersections, silicification halos, and Au + Cu geochemical anomalies, consistent with established controls on intrusion-related gold mineralization [11, 15]. The close alignment between high-confidence (low-uncertainty) targets and key geological features validates the reliability of the approach. By distinguishing Tier-1 (high-prospectivity, low-uncertainty) drill-ready targets from Tier-2 areas requiring additional data, the methodology significantly improves exploration efficiency and reduces risk in complex terrains. Overall, the DAE–UQ framework provides a scalable, uncertainty-aware tool for data-driven 3D ore prospectivity modeling in structurally complicated metallogenic systems. It holds strong potential for application to other deposit types and for incorporation of emerging datasets, such as hyperspectral remote sensing [2, 8, 9].

Declaration of Competing Interests

The authors declare no competing interests.

Funding

No funding was received for this study.

Data Availability

The datasets generated and analyzed during this study are available from the corresponding author upon reasonable request.

References

[1]. Carranza, E., Hale, M., & Faassen, C. (2008). Selection of coherent deposit-type locations and their application in data-driven mineral prospectivity mapping. *Ore Geology Reviews, 33*(3-4), 536-558.

[2]. Zuo, R., Yang, F., Cheng, Q., & Kreuzer, O. P. (2024). A novel data-knowledge dual-driven model coupling artificial intelligence with a mineral systems approach for mineral prospectivity mapping. *Geology*.

[3]. Zhang, Z., Li, Y., Wang, G., Carranza, E. J. M., Yang, S., Sha, D., Fan, J., Zhang, X., & Dong, Y. (2023). Supervised mineral prospectivity mapping via class-balanced focal loss function on imbalanced geoscience datasets. *Mathematical Geosciences, 55*(8), 989-1010.

[4]. Hronsky, J. M. A., & Groves, D. I. (2008). Science of targeting: Definition, strategies, targeting and performance measurement. *Australian Journal of Earth Sciences, 55*(1), 3-13.

[5]. Li, Q., Chen, G., & Luo, L. (2023). Mineral prospectivity mapping using attention-based convolutional neural network. *Ore Geology Reviews, 156*, 105381.

[6]. Daviran, M., Maghsoudi, A., & Ghezelbash, R. (2025). Optimized AI-MPM: Application of PSO for tuning the hyperparameters of SVM and RF algorithms. *Computers & Geosciences, 195*, 105785.

[7]. Bonham-Carter, G. F. (1994). *Geographic information systems for geoscientists: Modelling with GIS*. Pergamon Press.

[8]. Farhadi, S., Tatullo, S., Boveiri Konari, M., & Afzal, P. (2024). Evaluating StackingC and ensemble models for enhanced lithological classification in geological mapping. *Journal of Geochemical Exploration, 260*, 107441. https://doi.org/10.1016/j.gexplo.2024.107441

[9]. Pourgholam, M. M., Adib, A., Afzal, P., Rahbar, K., & Gholinejad, M. (2025). Deep learning and fractal-wavelet techniques for magnetite-apatite exploration in Tarom Iran. *Scientific Reports, 15*(1), 31907. https://doi.org/10.1038/s41598-025-16040-2

[10]. Liu, Z., Yu, S., Deng, H., Jiang, G., Wang, R., Yang, X., Song, J., Chen, J., & Mao, X. (2024). 3D mineral prospectivity modeling in the Sanshandao goldfield, China using the convolutional neural network with attention mechanism. *Ore Geology Reviews, 164*, 105861.

[11]. Uteshov, Y., Galiyev, D., Galiyev, S., Rysbekov, K., & Nauryzbayeva, D. (2021). Potential for increasing the efficiency of design processes for mining the solid mineral deposits based on digitalization and advanced analytics. *Mining of Mineral Deposits*.

[12]. Gal, Y., & Ghahramani, Z. (2016). Dropout as a Bayesian approximation: Representing model uncertainty in deep learning. *Proceedings of the 33rd International Conference on Machine Learning, 48*, 1050-1059.

[13]. Deng, H., Zheng, Y., Chen, J., Yu, S., Xiao, K., & Mao, X. (2022). Learning 3D mineral prospectivity from 3D geological models using convolutional neural networks: Application to a structure-controlled hydrothermal gold deposit. *Computers & Geosciences, 161*, 105074.

[14]. Li, R., Tan, S., Zhang, M., Zhang, S., Wang, H., & Zhu, L. (2024). Geological disaster susceptibility evaluation using a random forest empowerment information quantity model. *Sustainability, 16*(3), 765.

[15]. Goodfellow, I., Bengio, Y., & Courville, A. (2016). *Deep learning*. MIT Press.

[16]. Kingma, D. P., & Ba, J. (2015). Adam: A method for stochastic optimization. *International Conference on Learning Representations (ICLR)*.

[17]. Kendall, A., & Gal, Y. (2017). What uncertainties do we need in Bayesian deep learning for computer vision? *Advances in Neural Information Processing Systems, 30*, 5574-5584.

[18]. Cao, X., Liu, Z., Hu, C., Song, X., Quaye, J. A., & Lu, N. (2024). Three-dimensional geological modelling in earth science research: An in-depth review and perspective analysis. *Minerals, 14*(7), 686.

[19]. Heaton, J. (2018). [Review of the book *Deep learning*, by I. Goodfellow, Y. Bengio, & A. Courville]. *Genetic Programming and Evolvable Machines, 19*(1-2), 305-307. https://doi.org/10.1007/s10710-017-9314-z

[20]. Gal, Y., & Ghahramani, Z. (2016). Dropout as a Bayesian approximation: Representing model uncertainty in deep learning. *Proceedings of the 33rd International Conference on Machine Learning, 48*, 1050-1059.

[21]. Kingma, D. P., & Ba, J. (2015). Adam: A method for stochastic optimization. *International Conference on Learning Representations (ICLR)*.

[22]. Loshchilov, I., & Hutter, F. (2019). Decoupled weight decay regularization. *International Conference on Learning Representations (ICLR)*.

[23]. Srivastava, N., Hinton, G., Krizhevsky, A., Sutskever, I., & Salakhutdinov, R. (2014). Dropout: A simple way to prevent neural networks from overfitting. *Journal of Machine Learning Research, 15*(1), 1929-1958.

[24]. Rodriguez-Galiano, V., Sanchez-Castillo, M., Chica-Olmo, M., & Chica-Rivas, M. (2015). Machine learning predictive models for mineral prospectivity: An evaluation of neural networks, random forest, regression trees and support vector machines. *Ore Geology Reviews, 71*, 804-818.

[25]. Haghighi, A., Imamalipour, A., & Barak, S. (2025). Leveraging EDA, fractal analysis, SFA, and GMPI for identifying geochemical anomalies in Siah Cheshmeh ophiolite area, NW Iran. *Geopersia, 15*(1), 137-161.

[26]. Moghadam, H. S., Xiao, W., Dilek, Y., Ghorbani, G., Chiaradia, M., Santos, J. F., Ottley, C. J., Karsli, O., Khedr, M. Z., & Arai, S. (2025). Mineral, bulk rock, and isotope geochemistry of the Late Cretaceous Sabzevar ophiolite in NE Iran and the magmatic and tectonic evolution of a continental back-arc basin oceanic crust in the Mesozoic Tethyan orogenic belt. *Geological Society of America Bulletin, 137*(3-4), 649-681.

[27]. Aghazadeh, M., Castro, A., Badrzadeh, Z., & Vogt, K. (2015). Geochemistry and petrogenesis of intrusive plutons in the Urumieh-Dokhtar magmatic arc, Iran: Implications for subduction magmatism. *Journal of Asian Earth Sciences, 111*, 167-190.

[28]. Dentith, M., & Mudge, S. T. (2014). *Geophysics for the mineral exploration geoscientist*. Cambridge University Press.

[29]. Salarian, S., Oskooi, B., Mostafaei, K., & Smirnov, M. Y. (2024). Improving the resource modeling results using auxiliary variables in estimation and simulation methods. *Earth Science Informatics, 17*,

4161-4181. https://doi.org/10.1007/s12145-024-01383-7

[30]. Mostafaei, K., Maleki, S., Jodeiri Shokri, B., & Yousefi, M. (2023). Predicting gold grade by using support vector machine and neural network to generate an evidence layer for 3D prospectivity analysis. *International Journal of Mining and Geo-Engineering, 57*(4), 435-444.

[31]. Senge, R., Bösner, S., Dembczyński, K., Haasenritter, J., Hirsch, O., Donner-Banzhoff, N., & Hüllermeier, E. (2014). Reliable classification: Learning classifiers that distinguish aleatoric and epistemic uncertainty. *Information Sciences, 255*, 16-29.

[32]. Lakshminarayanan, B., Pritzel, A., & Blundell, C. (2017). Simple and scalable predictive uncertainty estimation using deep ensembles. *Advances in Neural Information Processing Systems, 30*, 6402-6413.

[33]. Kruse, F. A., Boardman, J. W., & Huntington, J. F. (2003). Comparison of airborne hyperspectral data and EO-1 Hyperion for mineral mapping. *IEEE Transactions on Geoscience and Remote Sensing, 41*(6), 1388-1400.

[34]. Blundell, C., Cornebise, J., Kavukcuoglu, K., & Wierstra, D. (2015). Weight uncertainty in neural networks. *Proceedings of the 32nd International Conference on Machine Learning, 37*, 1613-1622.

انجمن مهندسی معدن ایران
نشریه مهندسی معدن و محیط زیست
نشانی نشریه: www.jme.shahroodut.ac.ir
دانشگاه صنعتی شاهرود

مدل‌سازی پتانسیل معدنی سه‌بعدی با استفاده از رمزگذار خودکار عمیق همراه با سنجش عدم قطعیت: مطالعه موردی از شمال غرب ایران

عباس بحرودی* و سلمان فراهانی

دانشکده مهندسی معدن، دانشگاه تهران، تهران، ایران

اطلاعات مقاله

تاریخ ارسال: ۲۰۲۵/۱۱/۱۶
تاریخ داوری: ۲۰۲۵/۱۲/۱۳
تاریخ پذیرش: ۲۰۲۶/۰۲/۱۴

DOI: 10.22044/jme.2026.17156.3393

کلمات کلیدی

مدل‌سازی پتانسیل معدنی سه‌بعدی
رمزگذار خودکار عمیق
سنجش عدم قطعیت
کانسار طلای مرتبط با توده نفوذی سیه‌چشمه

چکیده

کاهش روزافزون ذخایر معدنی نزدیک‌سطح و افزایش پیچیدگی محیط‌های زمین‌شناسی در عمق، نیاز به چارچوب‌های داده‌بنیان سه‌بعدی در اکتشاف کانسارها را ضروری‌تر ساخته است. این پژوهش، یک روش یکپارچه مدل‌سازی پتانسیل معدنی سه‌بعدی را ارائه می‌دهد که یک رمزگذار خودکار عمیق را با سنجش عدم قطعیت مبتنی بر روش حذف تصادفی مونت‌کارلو ترکیب کرده تا هم برآوردهای دقیق پتانسیل معدنی و هم سنجه‌های اطمینان از مدل را تولید کند. داده‌های چندمنبعی زمین‌شناسی، زمین‌شیمی، ژئوفیزیک و گمانه‌های اکتشافی از سامانه طلای مرتبط با توده نفوذی سیه‌چشمه در شمال‌غرب ایران، در یک شبکه یکپارچه سه‌بعدی سازماندهی شد. ساختار چندمقیاسی رمزگذار خودکار عمیق، به‌خوبی الگوهای پنهان فضایی مربوط به زون‌های دگرسانی، برخوردهای ساختاری و ناهنجاری‌های ژئوفیزیکی را شناسایی کرد، درحالی‌که ۵۰ بار اجرای احتمالی با روش حذف مونت‌کارلو، امکان تفکیک عدم قطعیت ذاتی و عدم قطعیت مدل را فراهم آورد. مدل پیشنهادی به دقت ۸/۹۶ درصد و سطح زیر منحنی عکس‌العمل ۹۶/۰ دست یافت و عملکرد مدل‌های رمزگذار خودکار معمولی، شبکه عصبی کانولوشنی و جنگل تصادفی را ۴ تا ۵ درصد بهبود بخشید. مناطق با پتانسیل معدنی بالا (بیش از ۷۲/۰) تنها ۲۴ درصد از حجم مطالعه را پوشش دادند، اما ۶۸ درصد از بخش‌های معدنی شده در گمانه‌ها را شامل شدند. تحلیل عدم قطعیت، افزایش عدم اطمینان در مرزهای مناطق فاقد داده کافی را نشان داد و حذف بلوک‌های با عدم قطعیت بالا، دقت پیش‌بینی را به ۶/۹۸ درصد رساند. هم‌خوانی فضایی میان بلوک‌های پربازده، ناهنجاری‌های طلا و مس، هاله‌های سیلیسی شدن و سامانه‌های گسل ترافشار، اعتبار زمین‌شناسی خروجی‌های مدل را تأیید می‌کند. در مجموع، این چارچوب پیشنهادی، راه‌حلی مقیاس‌پذیر و آگاه از عدم قطعیت برای تحلیل پتانسیل معدنی سه‌بعدی در زمین‌های معدنی با ساختار پیچیده ارائه می‌دهد. توانایی تعمیم‌پذیری و استواری بالای آن، امکان به‌کارگیری این روش را برای دیگر انواع کانسارها و مجموعه‌داده‌های نوین زمین‌شناسی فراهم می‌سازد.

نویسنده مسئول مکاتبات: bahroudi@ut.ac.ir (ع. بحرودی)